RMI-chip: a microfluidics setup for functional imaging of microbial interactions with tree roots

Marie-Francoise S. Gros[a], Shalaka V. Shinde[a,†], Chase Akins[a], Jessica L. Johnson[a], Sarah Zerbs[a], Rosemarie Wilton[a], Ken Kemner[a], Philippe Noirot[a], Gyorgy Babnigg[a]*

Abstract

Coupling microfludics with microscopy has emerged as a powerful approach to study dynamics in plant physiology at cellular resolution and at higher throughput than with conventional methods. Most devices have been designed to study the model plant *Arabidopsis thaliana*, including root-microbe interactions. However, there is a need for microfluidic devices which enable *in vivo* studies of root development and root-microbe interactions in woody plants. Here, we developed the RMI-chip, a microfluidic setup that allows for continuous microscopic scale observation of real-time interactions between live *Populus tremuloides* (aspen tree) seedling roots and the rhizobacterium *Pseudomonas fluorescens* over an extended period longer than a month. Colonization dynamics in the RMI-chip are consistent with previous observations in a different experimental set-up. Also, we find that biosensors based on the rhizobacterium *Bacillus subtilis* can be used to monitor compositional changes in root exudates but that their application is limited by their inefficient colonization of aspen roots. Our results indicate that functional imaging of dynamic root-bacteria interactions in the RMI-chip requires careful matching between the host plant and the bacterial root colonizer.

Introduction

24 The plant microbiome plays an important role in the rhizosphere [1-3]. Virtually all plant tissues host
25 microbes that can act as symbionts, commensals, or pathogens. Interactions between plant and microbes
26 can be beneficial, neutral, or harmful and directly influence plant growth and productivity [2, 4, 5]. Plant-
27 growth-promoting (PGP) rhizobacteria are bacteria that exert beneficial effects on plants through direct
28 or indirect interactions with the roots [6, 7]. PGP bacteria have the potential to increase the availability of
29 soil nutrients to the plant, produce metabolites such as plant hormones, elicit plant systemic defences,
30 and increase plant resistance to biotic and abiotic stresses [8, 9]. In return, the plant provides
31 photosynthetically-derived carbon, such as sugars and organic acids that are consumed by rhizosphere
32 microorganisms as well as a wide range of molecular compounds acting as environmental signals for the
33 root microbiota. Microbes attach to the root surface and form microcolonies that can eventually grow
34 into larger biofilms. The formation of biofilms at root surfaces was proposed to be part of the cellular PGP
35 activities of beneficial rhizobacteria [10].
36 Understanding these complex interactions between plant roots and microbes requires the ability to track
37 their dynamics at high spatial and temporal resolution. Real time monitoring of dynamic root-microbe
38 interactions at cellular resolution is now possible using microfluidics approaches coupled with advanced
39 live imaging microscopy. Microfluidic platforms provide a powerful approach to evaluate the responses
40 of growing plant cells to external perturbations (e.g., nutrients, media flow, temperature, hydrodynamics,
41 light, and stressors) at throughputs higher than with conventional methods using pots or plates, and in
42 precisely controlled environments. Multiple microfluidics devices such as “Plant on a chip” [11], RootChip
43 [12], RootArray [13], TipChip [14], and PlantChip [15] were developed to study various aspects of the cell
44 biology of *Arabidopsis thaliana*, including gene expression, cell biomechanics, cellular mechanism of
45 growth and cell division (reviewed in [16]). The PlantChip device enables the continuous monitoring of
46 phenotypic changes at the cellular level and also at the whole plant level, including seed germination and
47 root and shoot growth (hypocotyls, cotyledons, and leaves) [15].

48 Fewer studies have used microfluidic devices to visualize the interactions of *Arabidopsis* roots with
49 pathogenic or beneficial microorganisms. Using the plant-in-chip platform, visualization of the attack of
50 *Arabidopsis* roots by pathogenic nematodes and oomycetes motile spores revealed some physiological
51 changes taking place in the host plant and the pathogen during the attack [17]. Recently, a microfluidic
52 device to track root interactions system (TRIS) revealed a distinct chemotactic behaviour of the bacterium
53 *Bacillus subtilis* toward the root elongation zone and its rapid colonization, and allowed real-time
54 monitoring of bacterial preference between roots from various *Arabidopsis* genotypes [18]. To date,
55 studies of plant roots and root-microbe interactions (RMIs) using microfluidics have been focused on *A.*
56 *thaliana*, an annual herbaceous plant model that can complete is entire life cycle in 6 weeks, and grows a
57 single primary root that later produces smaller lateral roots. However, there is a need to study root
58 development and root-microbe interactions for other plants, including woody perennial plants such as
59 trees.
60 Here, we describe a microfluidic device, called RMI-chip, that enables the direct visualization of root-
61 microbe interactions taking place at early stages of tree seedling growth. We studied the interactions of
62 *Populus tremuloides* (trembling aspen tree) with the bacterium *Pseudomonas fluorescens.* These
63 interactions are biologically relevant in nature, as *P. fluorescens* is abundant in the rhizosphere of *Populus*
64 trees [1, 19-21], and exhibits functionality in laboratory assays. We have shown that *P. fluorescens*
65 promotes the growth of aspen seedlings [22], colonizes aspen seedling roots by forming dense and
66 dynamic biofilms [23], and modulates expression of anti-fungal defence response genes in roots of aspen
67 seedlings [24]. The RMI-chip device was designed to accommodate aspen seedling growth for periods up
68 to 5 weeks, and to enable direct observation of root growth and its dynamic colonisation by *P. fluorescens*
69 biofilms with high spatiotemporal resolution. The RMI-chip was also used to monitor the growth of rice
70 seedling roots and detect the production of reactive oxygen species (ROS) by the root using engineered
71 *Bacillus subtilis* strains as biosensors. We find that in the RMI-chip interactions between host plants and

72 bacterial species are specific, consistent with ecological observations and with colonization profiles
73 observed in other experimental systems, and that formation of bacterial biofilms on root surfaces is
74 needed for extended colonization.
75
76 **Experimental**
77
78 **Materials and chemicals**
79
80 Seeds of Populus tremuloides Michx. were obtained from the National Tree Seed Center, Natural
81 Resources Canada, Fredericton NB, Canada. The rice seeds were obtained from Baker Creek Heirloom
82 Seed Co. (Mansfield, MO, USA). Phytoblend was purchased from Caisson Laboratories, Inc. (Smithfield,
83 UT, USA). All other chemicals were purchased from Sigma-Aldrich (St. Louis, MO, USA).
84
85 **RMI-chip and humidity chamber design**
86
87 The chips were designed with AutoCAD software (Autodesk) and were fabricated via soft lithography at
88 the Scientific Device Laboratory (Des Plaines, IL, USA). Briefly, SU-8 2025 photoresist (MicroChem,
89 Westborough, MA, USA) was used to make moulds on a 4-inch silicon wafer. The two-part silicone
90 elastomer (SYLGARD 184, Thermo Fisher Scientific, Waltham, MA), the silane precursor and curing agent
91 were mixed 10:1, degassed, poured on silicon wafer mould, degassed and baked at 65 °C for 4 hours. The
92 PDMS elastomer was punched and bonded to a 48 x 65mm, thickness No. 1 cover glass (Ted Pella Inc.,
93 Redding, CA, USA). RMI-chip devices were used without Aquapel treatment. The humidity chambers and
94 microscope stage adapters were fabricated from PMMA thermoplastic via laser cutting (Ponoko, Oakland,
95 CA, USA) and assembled with acrylic adhesive (Weld-On, Compton, CA, USA). Tubing management and

96 other holder accessories were 3D printed using PLA. The AutoCAD files (ESI) of the RMI-chip design, the
97 SVG files used for laser cutting, and the SCAD and STL files used for 3D printing are available in the online
98 supporting material.
99
100 **Fluorescent-labelled and biosensor bacterial strains**
101
102 The mNeonGreen (mNG)- and dsRed-labelled *P. fluorescens* SBW25 strains harboured an environmentally
103 stable plasmid derivative that constitutively expresses the dsRed or mNG fluorescent proteins, as
104 described [25]. *B. subtilis* strains labelled with the mCherry fluorescent protein were constructed by
105 transferring the genetic construct P_{pen}-mCherry::*kan* from *B. subtilis* MMB1023 [26] into the NCIB3610
106 background by phage transduction. The resulting NCIB3610-mcherry strain, which expressed
107 constitutively mCherry, was used as a recipient for the transfer of sensory genetic elements. A xylose-
108 responsive genetic module was constructed by inserting a P_{xylA} BioBrick DNA block (PCR-amplified from
109 plasmid pBS1C3-PxylA) into plasmid pBS1C [27] to form pBS1C-PxylA, which was then used as recipient
110 for the insertion of the gfp_{sp} gene from pRD111 [28], using Spe1 and Pst1 restriction sites. In the final
111 plasmid pBS1C-P_{xylA}-gfp_{sp}, the gfp_{sp} gene is under control of the xylose-inducible P_{xylA} promoter, linked with
112 a chloramphenicol resistance gene (*cat*) and flanked by the right and left arms of the *B. subtilis amyE* gene.
113 The P_{xylA}-GFP::*cat* module was integrated in the *amyE* gene of *B. subtilis* strain 1A976 (SKC6) by
114 transformation of the competent cells. The module was then finally transferred in the NCIB3610-mCherry
115 strain by SPP1-mediated phage transduction. A ROS-responsive *B. subtilis* strain was constructed by SPP1
116 transduction of the genetic module P_{katA}-gfp_{sp}::*spc* from strain 1A1010 (Bacillus Genetic Stock Center,
117 http://www.bgsc.org), where P_{katA} is the promoter controlling the expression the catalase gene, in the
118 NCIB3610 strain for integration at *amyE locus*. Transductants were selected for resistance to
119 spectinomycin.

120

121 **Aspen and rice cultivation**

122

123 *Populus tremuloides* Michx. seeds were cold stratified in Milli-Q water at 4°C for 2 to 14 days. Seeds were
124 then surface sterilized by prewashing briefly in 1% Tween-20 and incubated in pH-reduced (10 mM HCl)
125 0.1M sodium hypochlorite. After 4 minutes of incubation the seeds were rinsed 8-10 times with sterile
126 Milli-Q water and incubated in sterile Milli-Q water overnight in the dark at room temperature. The
127 following day the seeds were spread onto 1% agar Johnson's plate (4 mM KNO3, 2 mM Ca(NO3)2, 4 mM
128 NH4NO3, 0.5 mM KH2PO4, 1 mM MgSO4, 440 µM KCl, 250 µM H3BO3, 20 µM MnSO4, 20 µM ZnSO4, 5
129 µM CuSO4, 5 µM NaMoO4, 5 µM CoCl2, 200 µM Fe,Na-EDTA, pH 5.6, 1% Phytoblend). **T**he seeds were
130 incubated under low to medium light on a 16hr light/8hr dark period, maintaining the temperature below
131 30°C. Once germinated, seedlings with hypocotyls shorter than 5 mm were transferred into cut 200 µL
132 pipette tips filled with 1% Johnson's agar to let the root elongate gravitropically. For a typical experiment
133 20-25 pipette tips were inserted into Johnson's agar (1%) plates at a ~45° angle and incubated under the
134 same conditions (Fig. S1). Root growth was checked periodically. Six seedling-containing tips with roots
135 grown close to the end of the tips were mounted into the RMI-chip, which was incubated at a ~45° angle
136 to facilitate root infiltration.
137 De-hulled rice seeds (*Oryza sativa* 'Diamante-INIA') were dehulled and prewashed briefly in 1% Tween-
138 20, followed by incubation in pH-reduced (40 mM HCl) 0.4M sodium hypochlorite solution on a rocker for
139 15-20 minutes. The seeds were rinsed 7 times with Milli-Q water, plated on 1% Johnson's agar, and
140 incubated at 30°C in the dark for 48-72 hours. When germinated and the radical protrusions reached 3-
141 6mm, the seedlings were planted directly into cut 200 µL pipette tips filled with Johnson's solution already
142 inserted into the RMI-chip.

143 Following hypochlorite sterilization, all seed and seedling manipulations were performed in a laminar flow
144 hood, including mounting in the RMI-chip. Syringes, tubing, and adaptors were autoclaved prior to
145 connection to the chip to maintain sterility during the extended continuous perfusion.

146 Bacterial inoculations of the RMI-chips

147 Bacterial species were cultivated overnight in LB at their respective optimal temperature (i.e. 28°C for *P.*
148 *fluorescens,* 37°C for *B. subtilis*) in the presence of the appropriate antibiotic selection. Overnight cultures
149 of *P. fluorescens* SBW25-mNG and -DsRed strains were centrifuged, rinsed in PBS, and re-suspended in
150 PBS to OD_{600}=4. A 10µl aliquot of cell suspension was used for inoculation of aspen roots. Overnight
151 cultures of *B. subtilis* biosensor strains were diluted 100-fold and grown in LB up to mid-exponential phase
152 (OD600=0.4), rinsed with PBS and likewise adjusted to OD600=4 for the inoculation of the roots of aspen
153 and rice seedlings. After overnight incubation without flow, excess bacteria were washed away with
154 Johnson's solution at a flow of 0.2 µL/min for 2 hours, followed by continuous perfusion at 0.02 µl/min.
155 The outlet ports were connected to 200 µL pipette tips during inoculation, excess liquid was removed,
156 and ports were connected to independent lines to prevent cross-communication between the 100 µm x
157 800 µm channels (Fig. 1a) and with the external Johnson's solution overlay during perfusion. Note that in
158 theory, the RMI-chip can be washed and autoclaved after first use making the second set of 6 independent
159 channels are available for a new experiment. In this study, RMI-chips were used only once.

160

161 **Imaging experiments**

162

163 An inverted Nikon C2+ laser-scanning confocal microscope was used for imaging experiments (Nikon,
164 Melville, NY, USA). An Eclipse Ti-E inverted microscope equipped with perfect focus system, an automated
165 stage, and with 10x, 20x, and 100x objective lenses (CFI Plan Fluor 10X, NA 0.3, WD 16 mm; CFI Plan
166 Apochromat Lambda 20x, NA 0.75, WD 1.00 mm; CFI Plan Apo Lambda 100x, NA 1.5, WD 130 um,

167 respectively) was used for single image, time series, and z-stack acquisitions. Laser illumination emission
168 at 488 nm coupled with a 525/50-nm excitation filter was used to capture mNeonGreen fluorescence, and
169 laser illumination at 561 nm coupled with a 595/50-nm excitation filter was used to capture dsRed (*P.*
170 *fluorescens*) or mCherry (*B. subtilis*) fluorescence. The transmitted light was also detected to image
171 bacterial colonization in the context of the root structure. A custom holder was designed to provide access
172 of the objective to the RMI-chip and imaging chamber.
173
174 **Results and discussion**
175
176 RMI-chip design optimized for aspen seedling growth
177 The RMI-chip was designed to observe the growth and rhizobacterial colonization of aspen seedling roots
178 over extended periods of time. The aspen root system consists of a taproot from which smaller branch
179 roots emerge. When a seed germinates, the first root to emerge is the primary root which develops into
180 the taproot. With seedlings grown into agar-filled pipette tips (Fig. S1a), we observed that the primary
181 root quickly branched after exiting the tip (Fig. S1b). Thus, seedlings were inserted into the RMI-chip
182 shortly before the primary root reached the end of the pipette tip. Further development of the primary
183 root, including formation of branch roots, was not hampered by the pipette tip (Fig. S2a). In early studies,
184 we observed that the primary root readily entered the RMI-chip circular chamber (Fig. 1a), but we found
185 that a substantial part of the root system di not continue into the linear growth channel, instead growing
186 in circles, which caused the seedling to wither quickly. This problem was resolved by growing the seedlings
187 semi-gravitropically in a chip tilted at a 45° angle, submerged in Johnson's solution for up to a week, until
188 the root tip reached the media inlets in the growth channel (Fig. S2c). Under these conditions, most
189 primary roots entered the growth channel, at which point the RMI-chip was placed horizontally in a
190 humidity chamber and continuous media flow was supplied (Fig. 2). Regular exchange of the nutrient

solution surrounding the RMI-chip and the maintenance of water-saturated paper used to provide the required humidity in the growth chamber, were crucial to obtain healthy seedling growth.

The RMI-chip has 6 independent channels with one inlet for the seedling root, two dedicated inlets with filters for media and bacterial inoculation, and one common outlet (Fig. 1 a). The features are generated via soft lithography on a silicon wafer, which is then used as a mould to produce polydimethylsiloxane (PDMS) slabs. The PDMS is bonded to a large thin microscope coverslip providing a means for imaging at cellular resolution using a confocal microscope. Different channel depths were tested for aspen seedling growth. Although aspen primary root can grow into an 80 µm x 80 µm channel in a submerged microfluidic device (Fig. S2b), the root occupied the entire channel precluding flow experiments. Therefore, we selected a channel width of 800 µm and fabricated channels with depths of 100 µm and 400 µm. While aspen seedlings grew similarly in both devices, the 400 µm deep channel did not position the root close to the glass coverslip, making it suboptimal for microscopic observations using objectives with standard working distances (Fig. 2). Our final design has growth channels 100 µm deep, 800 µm wide and 36 mm long, which can easily accommodate aspen primary roots and enable root growth under constant perfusion. Flow characteristics of the 400 µm x 800 channel were measured with fluorescently labelled styrene beads (Fig. 1b). Without perfusion, slight bulk material movement was detected. At 1 µL/min, laminar flow was observed with a measured 50 µm/s bead velocity (Supplementary video 1).

It can be challenging for plant roots to grow under constant flow. For example, without flow in a growth channel, root border cells and mucilage can be observed at the root tip (Fig. S2c, Fig. S3). These cells and mucilage can be washed away at high flow rates (e.g., 2 µL/min). Nevertheless, nutrient flow is needed to maintain seedling growth in the RMI-chip. Therefore, we determined a minimal flow rate of nutrient solution that did not affect root growth, preserving root morphology, including root cap, root hairs and mucilage, while keeping out air bubbles. After several iterations, each including at least 4 seedlings, the minimal flow rate was found to be 0.02 µL/min. As each channel is connected to an individual 1 ml syringe,

215 this flow rate provides enough media for up to 5 weeks. Under these conditions, the calculated average
216 laminar flow is 4 µm/s and the media is replaced every ~14 minutes in each channel. Aspen seedlings
217 exhibited a high heterogeneity in primary root growth with an average growth rate of 1 ± 0.9 mm/d. This
218 heterogeneity may be due to the use of open pollinated seeds which have different genetic makeups. In
219 addition, only 4 or 5 seedlings out of 6 mounted in the RMI-chip typically sustained growth over a 5-week
220 period. On average, aspen primary roots grew much slower than Arabidopsis primary roots reported to
221 grow at 3.7 mm/d in the RootChip [12].
222
223 **Continuous imaging of the RMI-chip**
224
225 Confocal Laser Scanning Microscopy was used to perform spatial and temporal studies of the aspen root
226 growth. Because of the repeated microscopy observations, a flexible system was required which was
227 compatible with the transfer of the chip between the growth chamber and microscope stage. A modular
228 chamber was designed to overcome this technical challenge and to prevent water evaporation during
229 cultivation and imaging. An innermost imaging chamber was built to provide humidity during the repeated
230 1-hour imaging experiments, and a medium-size chamber allowed submersion of the RMI-chip in media
231 and its transport between incubation chamber and microscope. A six-channel syringe pump was
232 connected with Teflon™ FEP tubing to the chip and transferred with the chip during imaging experiments
233 in order to provide continuous flow of nutrients, even during long imaging experiments (Fig. S4). Finally,
234 a large closed chamber that can be filled with water was built to provide humidity during long-term
235 growth. In addition, a holder compatible with the imaging chamber was fabricated for the Nikon Ti-2
236 microscope (Fig. S4). The humidity chambers and microscope stage adapters were fabricated from PMMA
237 thermoplastic. 3D printed inserts were fabricated to manage the tubing during imaging experiments
238 (design files are available in the online supporting material). With this system, the RMI-chip was

239 continuously perfused with Johnson's solution flowing at 0.02 µL/min, including during the lengthy
240 observations under the microscope, thus minimizing the disturbance of seedling growth.
241
242 **Growing rice seedlings in the RMI-chip**
243
244 We tested the compatibility of the RMI-chip with other plant species such as rice. Rice seedling roots could
245 be introduced easily into the chamber without an agar tip by directly transplanting the seedlings within
246 days after germination. Healthy root growth was observed under continuous perfusion with Johnson's
247 solution at a 0.02 µL/min flow rate (Fig. S5). Under these conditions, we observed fast root growth where
248 the root tip reached the end of growth chamber after 4 days on average. As for aspen, variability between
249 seedlings was observed, some root tips reaching RMI-chip end after 3.5 to 5 days. Thus, rice root growth
250 rate is approximately 10 times faster than aspen root growth under the same conditions. Unfortunately,
251 the fast growth rate of rice seedlings limits observation time to 3-5 days. Once the root tip reaches the
252 outlet, it blocks the chamber and cuts off nutrient flow.
253
254 **Colonization of aspen seedling root by *P. fluorescens***
255
256 Aspen seedlings grown for 8 days in the RMI-chip were inoculated with mNeonGreen-labelled *P.*
257 *fluorescens* SBW25 by injection of approximately 2 x 10^9 cells through an inlet port (Fig. S6a). After
258 incubation for 16 hours without flow, the flow was restored at 0.2 µL/min for 2 hours to wash away excess
259 bacterial cells, then set at 0.02 µl/min for continuous perfusion. Under these conditions, a small number
260 of SBW25 cells remained associated with the lower part of the root (Fig. S6b). Importantly, the only source
261 of carbon available for bacterial growth in the RMI-chip are the sugars and organic acids
262 photosynthetically produced by the plant. Five days after inoculation, actively dividing SBW25 cells were

263 colonizing the intercellular spaces between root epidermal cells of the root cortex, and, to a lesser extent,
264 the root surface (Fig. S7). Although this preferential colonization of crevices on the root surface may be
265 caused by the flow in the RMI-chip, it is consistent with our previous observations in a vertical plate
266 system, where SBW25 first colonizes the cell interstitial spaces along the aspen root cortex before forming
267 a variety of bacterial assemblies that range from microcolonies to highly structured biofilms [23].
268 Next, we observed aspen primary root colonization by a 1:1 mixture of two *P. fluorescens* SBW25
269 derivatives labelled with distinct fluorescent proteins, mNeonGreen and dsRed. Three days after
270 inoculation, we observed discrete patches of red and green cells with almost no area of mixed colours
271 (Fig. 3a). This finding indicates that bacterial cells divide and form expanding patches in the intercellular
272 spaces and on the root surface, ruling out that those patches are formed by random deposition and
273 aggregation of cells within the root crevices. Thirteen days after inoculation, bacterial patches were longer
274 and formed dense cell assemblies on the primary root surface (Fig. 3b). Close-up examination revealed
275 mature biofilms resulting from clonal growth of green and red bacterial populations. These biofilms
276 exhibited channel-like void spaces, which are a hallmark of mature biofilms [29]. Although cell density and
277 presence of small aggregates in the pure cultures prior to co-inoculation could play a role in determining
278 the colonisation patterns [30], the quasi-absence of intermixed biofilms is indicative of a competition
279 between the green and red strains. These strains have an identical genome but differ by the expressed
280 fluorescent protein, possibly creating differences in cell fitness and some competition.
281 Notably, we observed that a variety of SBW25 cell assemblies coexisted with biofilms on the root surface
282 (Fig. 4a). These assemblies included clusters of somewhat regularly spaced individual cells, clusters of cell
283 doublets which are presumably dividing, microcolonies and mature biofilms (Fig. S8). These assemblies
284 may reflect the different stages of biofilm formation, where cells attach to the root surface, divide, and
285 over time form more compact assemblies maturing into biofilms. Intriguingly, cells packed within a biofilm
286 appeared to have a round coccoid shape in contrast with the normal rod-like morphology of individual

287 SBW25 cells (Fig. 3a, Fig. 4a). Confocal 3D image reconstruction and side projection of the 3D volume (Fig.
288 4b) revealed that the coccoid shape was only apparent and resulted from the top view of vertically
289 arranged bacterial cells within the biofilm. This finding corroborates our previous observation of vertical
290 arrangements of SBW25 cells within biofilms and mucilage formed on the roots of aspen seedlings
291 growing in a vertical agar plate [23].
292 After 30 days in the RMI-chip, fluorescent SBW25 cells became rare on the root surface and were
293 preferentially found as micro-colonies located within the spaces between root epidermal cells (Fig. S9).
294 Overall, the dynamic of root colonization by SBW25, which includes active growth and colonization of the
295 root during the first two weeks, formation of mature biofilms associated with a variety of other cell
296 assemblies, and dispersal of these biofilms and assemblies after 5 weeks, appears to be remarkably
297 comparable in the RMI-chip and vertical plate assay, the latter being a very different set-up where seedling
298 roots grow on a nutrient agar surface [23]. This similarity suggests that the observed dynamics of cell
299 assemblies are not primarily shaped by the flow in the RMI--chip but rather reflect an intrinsic colonization
300 behaviour of aspen primary root by *P. fluorescens* SBW25. In addition, novel cell assemblies such as
301 clusters of somewhat regularly spaced individual cells and cell doublets were observed uniquely in the
302 RMI-chip.
303
304 **RMI-chip and rhizobacterial biosensors to monitor dynamic root exudation**
305
306 In the RMI-chip, the carbon sources available for bacterial growth are provided by root exudates. These
307 exudates are compositionally complex and contain ions (i.e. H+), inorganic acids, oxygen, water, and
308 multiple carbon-based compounds which include amino acids, organic acids, sugars, phenolics and an
309 array of secondary metabolites, and high-molecular weight compounds like mucilage and proteins [31].
310 Root exudates are key mediators of interactions with microbes in the rhizosphere and root exudation is a

311 regulated process which responds to biotic and abiotic stresses to the plant [31]. We assessed whether
312 biosensors, which are engineered rhizobacteria that can colonize root surfaces and express a fluorescent
313 protein in response to the presence of a specific metabolite or environmental stressor, could be used in
314 the RMI-chip to monitor dynamic changes in the composition of plant exudates.
315 We used *Bacillus subtilis,* which colonizes *Arabidospis* roots [18] and is used as biocontrol agent to colonize
316 and protect various herbaceous plants [32], to develop our biosensor strains. We selected two well
317 characterized promoters, one responding to the presence of xylose [33], a sugar abundant in root
318 exudates, and the other one responding to the presence of Reactive Oxygen Species (ROS) [34], which are
319 normal products of plant cellular metabolism and act as second messengers in plant responses to various
320 environmental stresses [35]. The biosensors expressed the green fluorescent protein (GFP) conditionally
321 in the presence of xylose or ROS and also expressed constitutively the red fluorescent protein mCherry,
322 which serves to label the cells (see Experimental methods).
323 Aspen primary roots were inoculated with *B. subtilis* biosensors in the RMI-chip, incubated overnight
324 without flow, and upon restoration of flow the root was observed using confocal laser microscopy. We
325 found that, as with *P. fluorescens*, most cells were rapidly washed away from the root surface. However,
326 biosensor cells were very sparse on the root after 3 days and could not be observed after 5 days. The use
327 of a low flow (0.02 µL/min) throughout inoculation of the RMI-chip did not enhance the number of
328 biosensor cells remaining attached to the primary root, reflecting an inability of *B. subtilis* to colonize
329 aspen primary root under these conditions. This is in contrast with our observations with *P. fluorescens*
330 and may reflect the fact that *B. subtilis* is not a natural colonizer of aspen roots. To circumvent this
331 problem, observations were done in a stopped-flow experiment limited to 5 days, after which the aspen
332 seedling starts to whither. Even In the absence of flow, *Bacillus* cells did not colonize but remained loosely
333 attached to the aspen root surface. Whereas biosensor cells did not express GFP after inoculation (Fig. 5
334 a), strong GFP signals were detected in biosensor cells remaining attached to the aspen root after 5 days

335 of incubation, indicating the production of xylose (Fig. 5b) or ROS (Fig. 5c) by the root. Exposure of the
336 ROS biosensor to a rice primary root under the same RMI-chip conditions (i.e., no flow) resulted in a robust
337 colonization of the root and in high levels of GFP after 3 days (Fig. 5d). This finding indicates that high
338 levels of ROS are produced by rice primary root. Together, these results provide a proof-of-concept that
339 bacterial biosensors can be used in RMI-chip as a way to investigate the dynamic chemical crosstalk
340 between root and rhizobacteria.
341 We also inoculated rice seedlings with *P. fluorescens* SBW25 to test for ability to colonize in the RMI-chip.
342 Repeated trials showed that SBW25 cells were rapidly washed away from the root surface and remained
343 barely detectable under nutrient flow after one day (data not shown), suggesting an inability of *P.*
344 *fluorescens* SBW25 to colonize rice primary root under these conditions. This result was unexpected as
345 rice was shown to host *Pseudomonas* endophytes [36]. These observations clearly show that biosensors
346 need to be developed from bacterial isolates that efficiently colonize the roots of the plant host of
347 interest. What may seem to be a caveat for the development of biosensors is actually grounded in ecology
348 and evolution, as root exudates from a particular plant species are known to maintain and support a highly
349 specific diversity of microbes in the rhizosphere of this plant [31].
350
351 **Conclusions**
352
353 In summary, a microfluidic device and accessories were fabricated enabling the long-term cultivation of
354 aspen seedlings under constant flow and the study of root-microbe interactions through repeated
355 functional imaging of the system. The device enabled high-resolution imaging through the various phases
356 of aspen colonization by *P. fluorescens* SBW25 at the single bacterial cell level under continuous nutrient
357 flow. Different biofilm morphologies and diverse bacterial assemblies were observed over time,
358 emphasizing the need for high-resolution imaging to understand colonization patterns and strategies over

359 time driven by local environments. *B. subtilis* biosensors provided a means for functional imaging of root
360 exudate uptake by the bacteria and the detection of an environmental stressor. However, the use of these
361 biosensors was limited by their lack of long term colonization of the host plant. The RMI-chip can be used
362 for the long-term observation of other slow-growing plants, or modified to study faster growing plants as
363 well.
364
365 **Conflicts of interest**
366
367 There are no conflicts to declare.
368
369 **Acknowledgements**
370
371 This work was performed under the Small Worlds project and was supported by the Office of Biological
372 and Environmental Research (BER), Office of Science, United States Department of Energy (DOE), under
373 Contract DE-AC02-06CH11357.
374
375 **Affiliation**
376
377 a. Argonne National Laboratory, Biosciences Division, 9700 S. Cass Ave., Argonne, IL 60439 USA.
378 † Current address: Oil-Dri Innovation Center, 777 Forest Edge Rd., Vernon Hills, IL 60061 USA.
379 * Corresponding author.
380 Electronic Supplementary Information (ESI) available: [AutoCAD files of the RMI-chip, SCAD files
381 of humidity chamber and microscope stage adapter, vector graphics of laser cut accessories, video
382 files of flow in microfluidic channel].

383 **Figures**

384

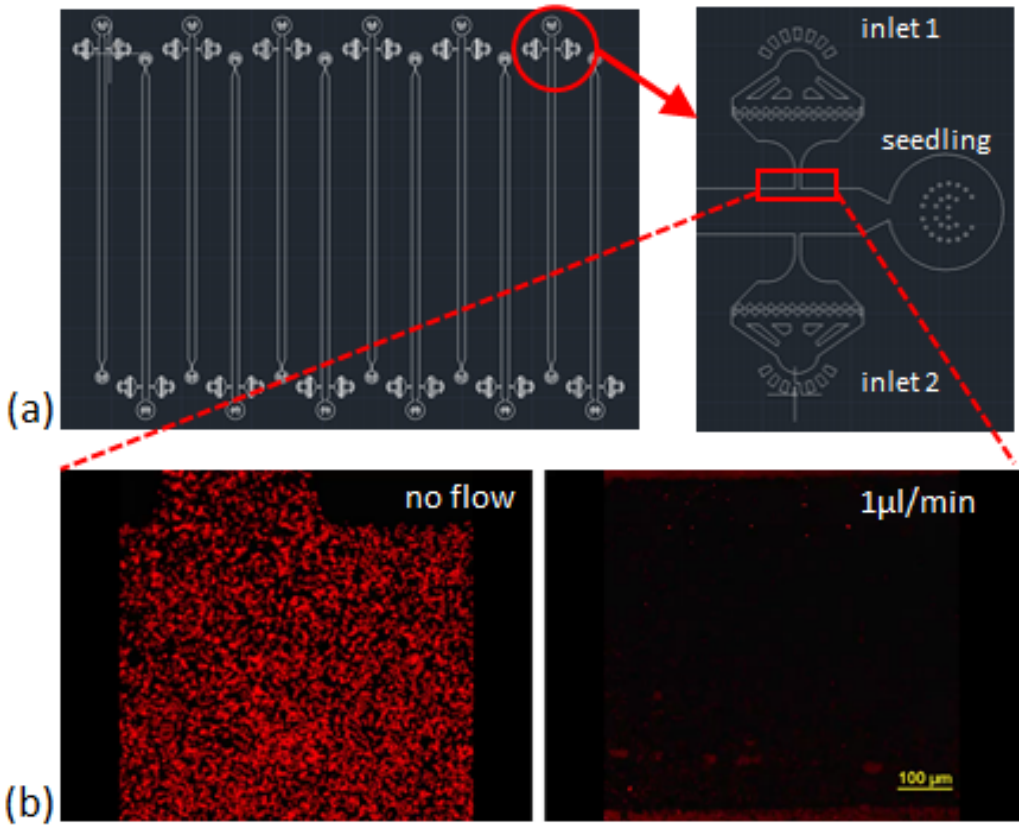

385

386 **Fig.1 RMI-chip design.** (a) The CAD design of the RMI-chip. A single growth channel is 36 mm long, 100
387 µm high, and 800 µm wide (a). The media and inoculation inlets are equipped with filters to avoid
388 occlusions during week-long experiments. Design files are available in the online supporting materials. (b)
389 Flow dynamics. Fluorescently labelled latex beads were used to measure media flow in the empty RMI-
390 chip. The root entrance and the inoculation inlets were plugged with stopper pins to mimic operational
391 flow regime of the chip. The latex beads suspended in Johnson were injected and the chip images,
392 followed by perfusion with Johnson solution at 1µL/min. The latex beads were washed from the upstream
393 chambers and the velocity of the beads were averaged. The measured and calculated values agreed.
394 Laminar flow was observed under the microscope.

395

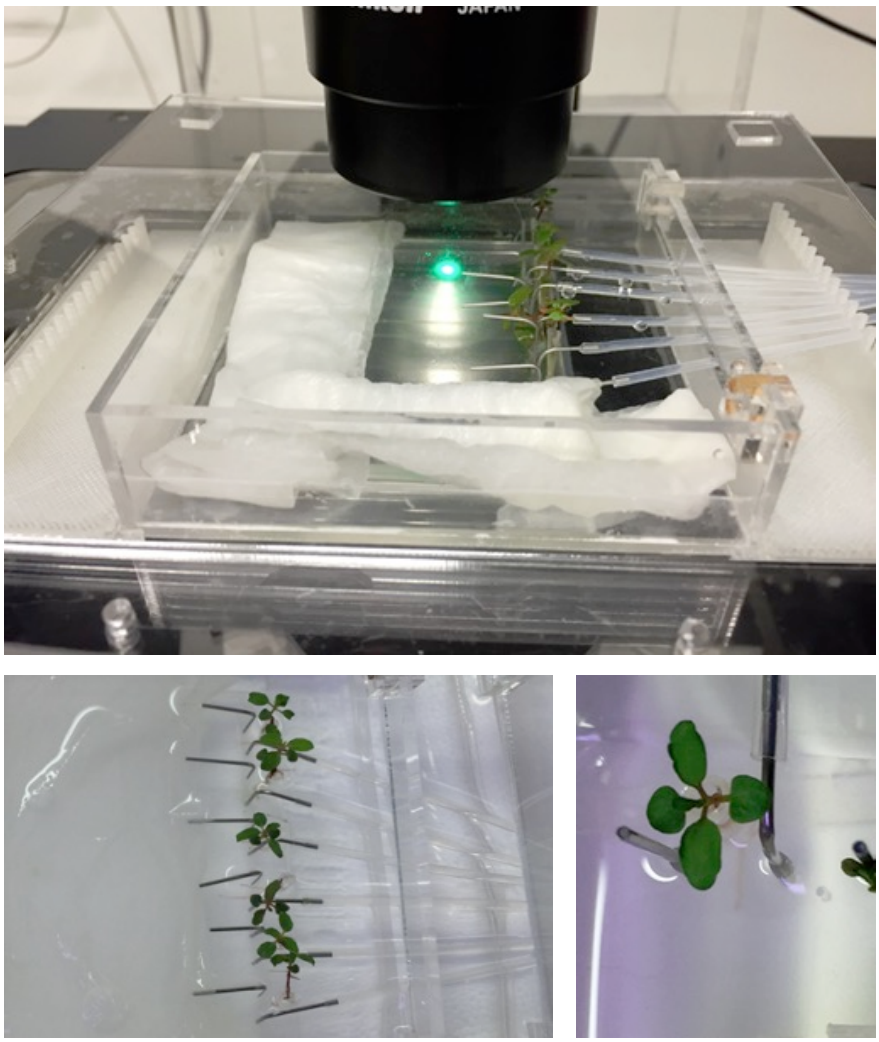

Fig. 2. Imaging setup. (a) The imaging setup with humidity chamber and 3D printed stage adaptor. The RMI-chip has an inlet for media, a separate port for inoculation, and a wide channel to accommodate the tree seedling root without interfering with constant media flow. (b) The continuous flow incubation chamber enables the cultivation of six seedlings in parallel (left). Details of an aspen seedling (right).

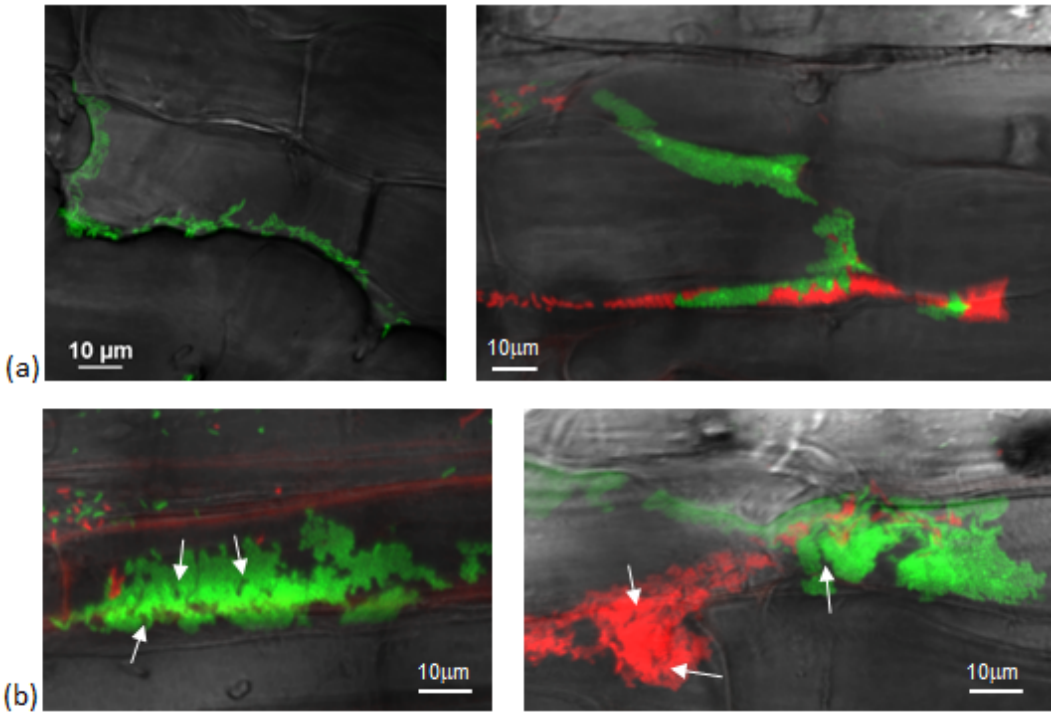

403

404 **Fig. 3. Spatial and temporal colonization of aspen primary roots by *P. fluorescens* in the RMI-chip:** *P.*

405 *fluorescens* SBW25 strains expressing dsRed or mNeonGeen were co-inoculated on aspen roots growing

406 in the RMI-chip. (a) After 3 days, bacterial cells colonize aspen root surface by filling intercellular spaces

407 (left panel) and adhering to plant cell surfaces (right panel). (b) After 13 days, SBW25 cells formed spatially

408 segregated red and green long patches of cells that correspond to dense biofilm-like assemblies. Typical

409 of mature biofilms, some internal void spaces and channels are indicated by arrows.

410

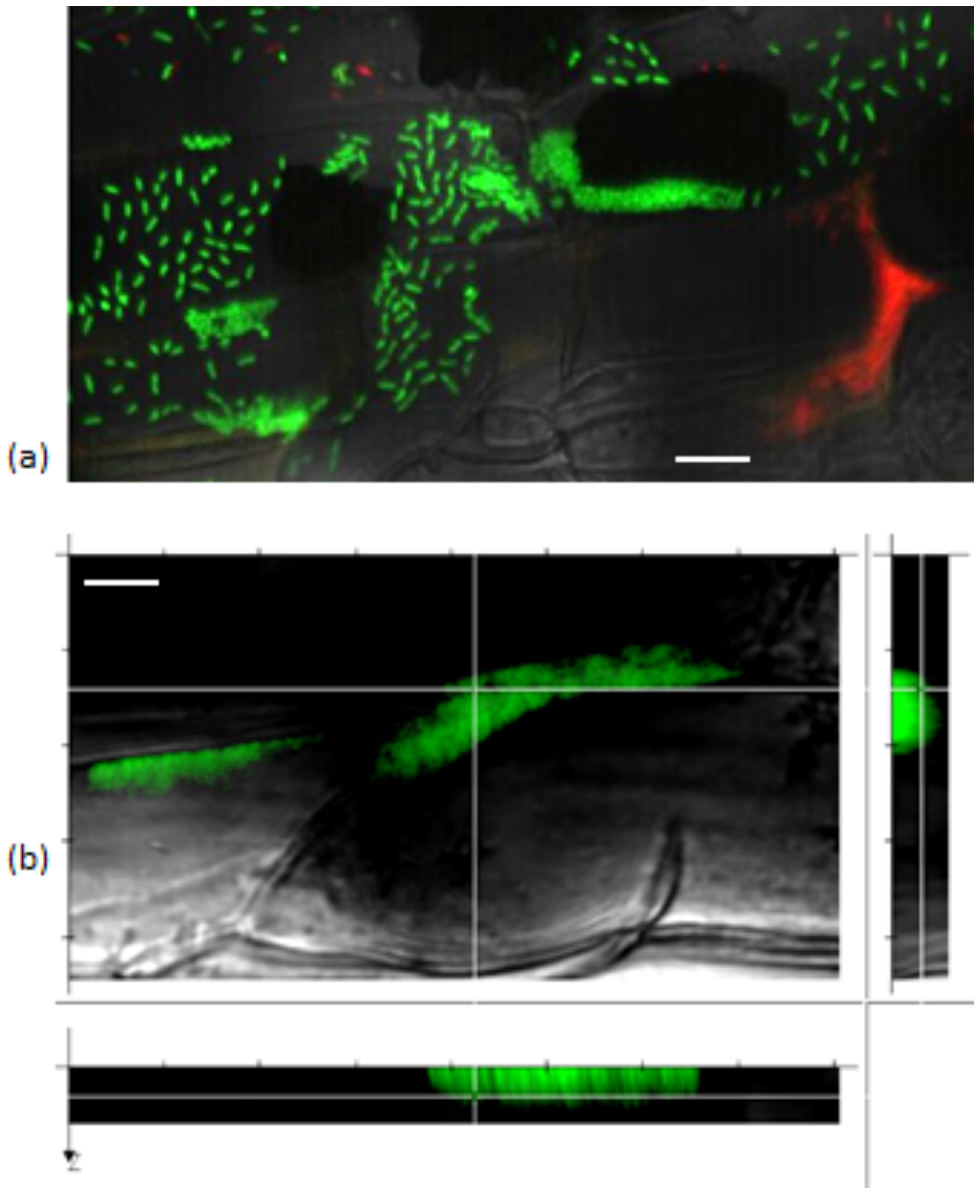

Fig. 4: A gallery of bacterial assemblies on the root surface. (a) Image showing diverse assemblies of green SBW25 cells on the root surface: 1, individual cells; 2, cell doublets; 3, microcolonies; and 4, biofilms. (b) Projection of a reconstructed 3D volume with side views reveals a vertical alignment of cells within the biofilm. Scale bar indicates 10 µm length.

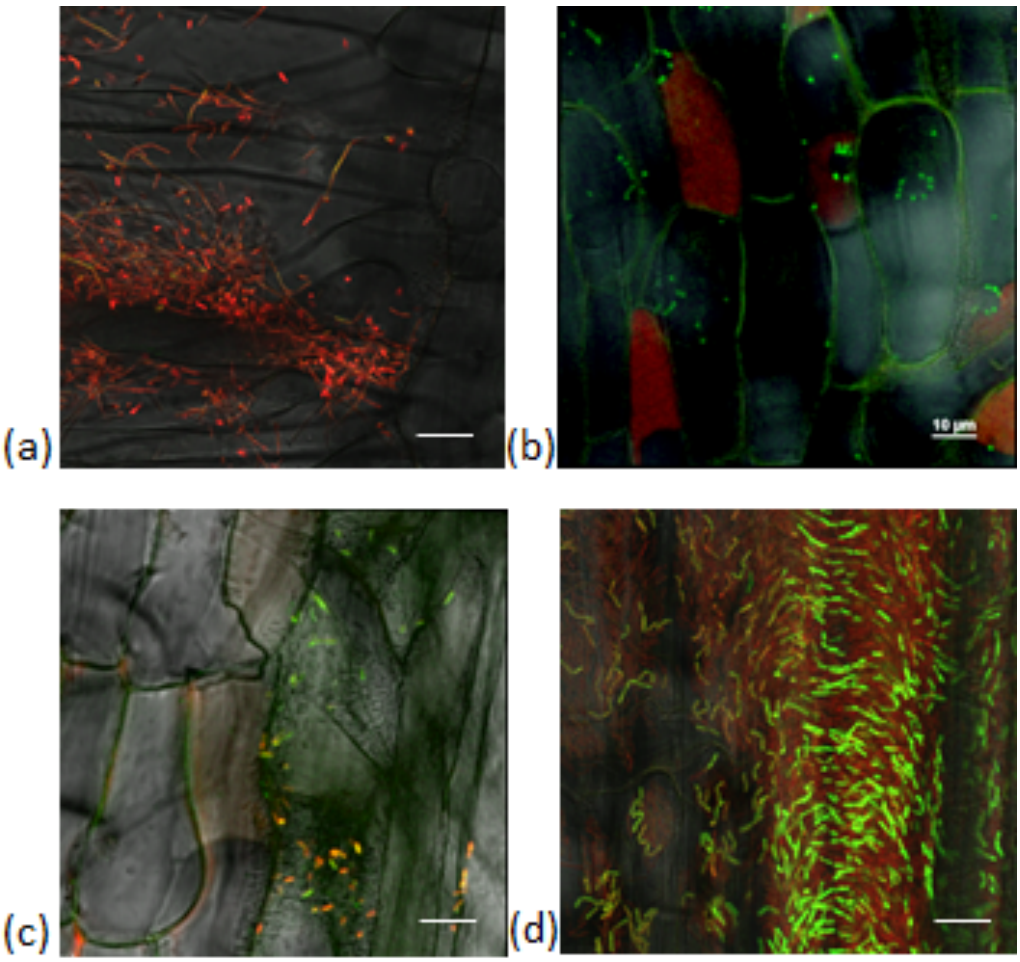

418

419 **Fig. 5. *B. subtilis* biosensors exposed to aspen root (panels a-c) and rice root (panel d) in the RMI-chip.**

420 (a) Among the root hairs, the xylose biosensor cells appear red from constitutive mCherry expression with

421 a very faint GFP (green) signal detected in some cells. Similar results were obtained with the ROS biosensor

422 (not shown). (b) Five days after inoculation, rare attached biosensor cells overwhelmingly express GFP,

423 indicating the presence of xylose in root exudates. Note the plant tissue autofluorescence causing cell

424 outlines to be green and some plant cells to be entirely red. (c) After 5 days, most ROS biosensor cells

425 expressed GFP, indicating the presence of ROS produced by the root. Plant tissue autofluorescence is also

426 detected. (d) Three days after inoculation of a rice seedling, the *B. subtilis* ROS biosensor displayed robust

427 colonization of the root with a strong expression of GFP, indicating production of ROS by the rice root.

428 Scale bar indicates 10 µm length.

429

430 **Notes and references**

431

432 1. Brown, S.D., et al., *Twenty-one genome sequences from Pseudomonas species and 19 genome*
433 *sequences from diverse bacteria isolated from the rhizosphere and endosphere of Populus deltoides.* J
434 Bacteriol, 2012. **194**(21): p. 5991-3.

435 2. Compant, S., et al., *Use of plant growth-promoting bacteria for biocontrol of plant diseases:*
436 *principles, mechanisms of action, and future prospects.* Appl Environ Microbiol, 2005. **71**(9): p. 4951-9.

437 3. Bulgarelli, D., et al., *Structure and functions of the bacterial microbiota of plants.* Annu Rev Plant
438 Biol, 2013. **64**: p. 807-38.

439 4. Newton, A.C., et al., *Pathogenesis, parasitism and mutualism in the trophic space of microbe-plant*
440 *interactions.* Trends Microbiol, 2010. **18**(8): p. 365-73.

441 5. Gaiero, J.R., et al., *Inside the root microbiome: bacterial root endophytes and plant growth*
442 *promotion.* Am J Bot, 2013. **100**(9): p. 1738-50.

443 6. Dupuy, L.X.a.S., W.K., *Mechanisms of Early Microbial Establishment on Growing Root Surfaces.*
444 Vadose Zone J. | Advancing Critical Zone Science, 2016. **15**(2).

445 7. Varivarn, K., et al., *Colonization strategies of Pseudomonas fluorescens Pf0-1: activation of soil-*
446 *specific genes important for diverse and specific environments.* BMC Microbiol, 2013. **13**: p. 92.

447 8. Barea, J.M., et al., *Microbial co-operation in the rhizosphere.* J Exp Bot, 2005. **56**(417): p. 1761-78.

448 9. Rodriguez, H. and R. Fraga, *Phosphate solubilizing bacteria and their role in plant growth*
449 *promotion.* Biotechnol Adv, 1999. **17**(4-5): p. 319-39.

450 10. Seneviratne G., W.M.L.M.A.W., Seneviratne K.A.C.N., Zavahir J.S., Kecskés M.L., Kennedy I.R. ,
451 *Importance of Biofilm Formation in Plant Growth Promoting Rhizobacterial Action*, in *Plant Growth and*
452 *Health Promoting Bacteria*, M. D., Editor. 2010, Springer, Berlin, Heidelberg: Berlin, Heidelberg.

453 11. Meier, M., E.M. Lucchetta, and R.F. Ismagilov, *Chemical stimulation of the Arabidopsis thaliana*
454 *root using multi-laminar flow on a microfluidic chip.* Lab Chip, 2010. **10**(16): p. 2147-53.
455 12. Grossmann, G., et al., *The RootChip: an integrated microfluidic chip for plant science.* Plant Cell,
456 2011. **23**(12): p. 4234-40.
457 13. Busch, W., et al., *A microfluidic device and computational platform for high-throughput live*
458 *imaging of gene expression.* Nat Methods, 2012. **9**(11): p. 1101-6.
459 14. Agudelo, C.G., et al., *TipChip: a modular, MEMS-based platform for experimentation and*
460 *phenotyping of tip-growing cells.* Plant J, 2013. **73**(6): p. 1057-68.
461 15. Jiang, H., et al., *Plant chip for high-throughput phenotyping of Arabidopsis.* Lab Chip, 2014. **14**(7):
462 p. 1281-93.
463 16. Sanati Nezhad, A., *Microfluidic platforms for plant cells studies.* Lab Chip, 2014. **14**(17): p. 3262-
464 74.
465 17. Parashar, A. and S. Pandey, *Plant-in-chip: Microfluidic system for studying root growth and*
466 *pathogenic interactions in Arabidopsis.* Applied Physics Letters, 2011. **98**(26).
467 18. Massalha, H., et al., *Live imaging of root-bacteria interactions in a microfluidics setup.* Proc Natl
468 Acad Sci U S A, 2017. **114**(17): p. 4549-4554.
469 19. Gottel, N.R., et al., *Distinct microbial communities within the endosphere and rhizosphere of*
470 *Populus deltoides roots across contrasting soil types.* Appl Environ Microbiol, 2011. **77**(17): p. 5934-44.
471 20. Timm, C.M., et al., *Metabolic functions of Pseudomonas fluorescens strains from Populus deltoides*
472 *depend on rhizosphere or endosphere isolation compartment.* Front Microbiol, 2015. **6**: p. 1118.
473 21. Weston, D.J., et al., *Pseudomonas fluorescens induces strain-dependent and strain-independent*
474 *host plant responses in defense networks, primary metabolism, photosynthesis, and fitness.* Mol Plant
475 Microbe Interact, 2012. **25**(6): p. 765-78.

476 22. Shinde, S., et al., *Pseudomonas fluorescens Transportome Is Linked to Strain-Specific Plant Growth*
477 *Promotion in Aspen Seedlings under Nutrient Stress.* Front Plant Sci, 2017. **8**: p. 348.
478 23. Noirot-Gros, M.F., et al., *Dynamics of Aspen Roots Colonization by Pseudomonads Reveals Strain-*
479 *Specific and Mycorrhizal-Specific Patterns of Biofilm Formation.* Front Microbiol, 2018. **9**: p. 853.
480 24. Shinde, S.Z., S.; Collart, RF.; Cumming, JR.; Noirot, P.; Larsen, P., *Pseudomonas fluorescens*
481 *increases mycorrhization and modulates expression of anti-fungal defense response genes in roots of*
482 *aspen seedlings.* BMC Plant Biology, in press.
483 25. Wilton, R., et al., *A New Suite of Plasmid Vectors for Fluorescence-Based Imaging of Root*
484 *Colonizing Pseudomonads.* Front Plant Sci, 2017. **8**: p. 2242.
485 26. Babic, A., et al., *Efficient gene transfer in bacterial cell chains.* MBio, 2011. **2**(2).
486 27. Radeck, J., et al., *The Bacillus BioBrick Box: generation and evaluation of essential genetic building*
487 *blocks for standardized work with Bacillus subtilis.* Journal of Biological Engineering, 2013. **7**(1).
488 28. Overkamp, W., et al., *Benchmarking Various Green Fluorescent Protein Variants in Bacillus subtilis,*
489 *Streptococcus pneumoniae, and Lactococcus lactis for Live Cell Imaging.* Applied and Environmental
490 Microbiology, 2013. **79**(20): p. 6481-6490.
491 29. O'Toole, G., H.B. Kaplan, and R. Kolter, *Biofilm formation as microbial development.* Annu Rev
492 Microbiol, 2000. **54**: p. 49-79.
493 30. Melaugh, G., et al., *Shaping the Growth Behaviour of Biofilms Initiated from Bacterial Aggregates.*
494 PLoS One, 2016. **11**(3): p. e0149683.
495 31. Badri, D.V. and J.M. Vivanco, *Regulation and function of root exudates.* Plant Cell Environ, 2009.
496 **32**(6): p. 666-81.
497 32. Allard-Massicotte, R., et al., *Bacillus subtilis Early Colonization of Arabidopsis thaliana Roots*
498 *Involves Multiple Chemotaxis Receptors.* MBio, 2016. **7**(6).

499 33. Kim, L., A. Mogk, and W. Schumann, *A xylose-inducible Bacillus subtilis integration vector and its*
500 *application.* Gene, 1996. **181**(1-2): p. 71-6.
501 34. Hoover, S.E., et al., *Changes in DnaA-dependent gene expression contribute to the transcriptional*
502 *and developmental response of Bacillus subtilis to manganese limitation in Luria-Bertani medium.* J
503 Bacteriol, 2010. **192**(15): p. 3915-24.
504 35. Sharma, P.J., A.B.; Dubey, R.S.; Pessarakli, M, *Reactive Oxygen Species, Oxidative Damage, and*
505 *Antioxidative Defense Mechanism in Plants under Stressful Conditions.* Journal of Botany, 2012. **2012**: p.
506 26.
507 36. Jha, Y. and R.B. Subramanian, *Characterization of root-associated bacteria from paddy and its*
508 *growth-promotion efficacy.* 3 Biotech, 2014. **4**(3): p. 325-330.
509

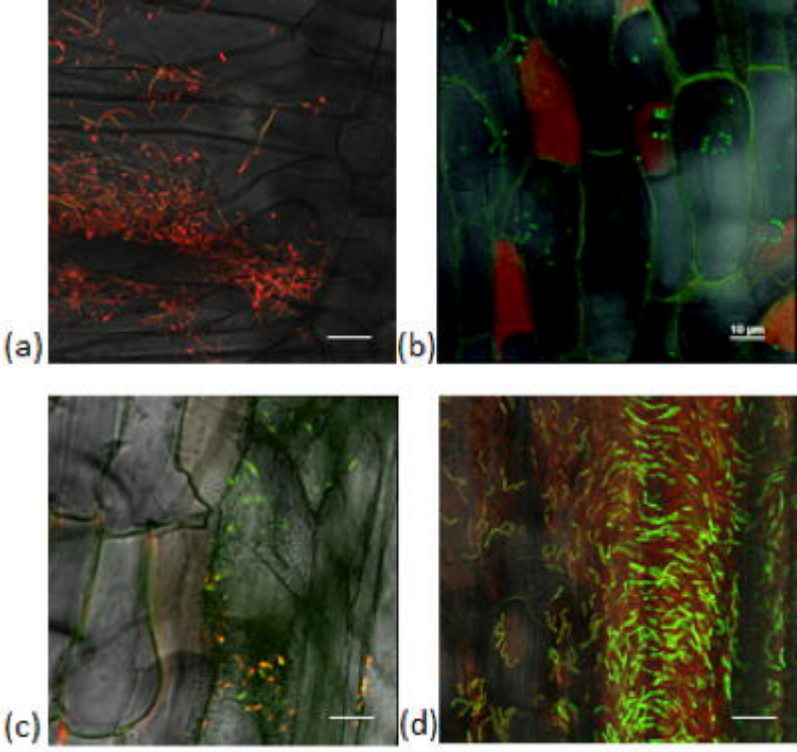
(a)
(b)
10 µm
(c)
(d)

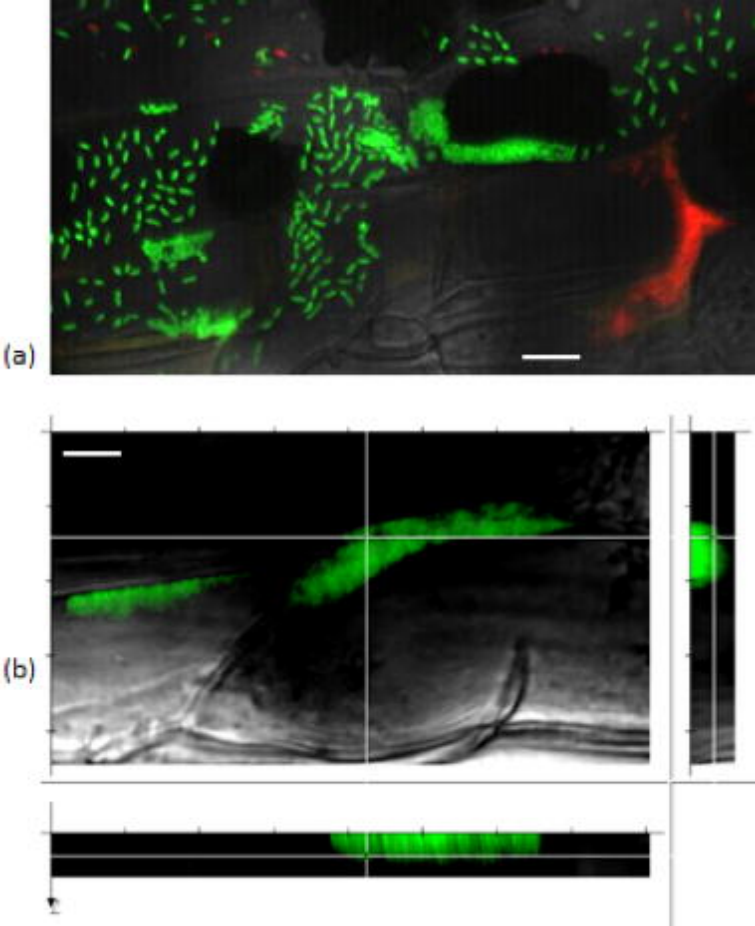
(a)
(b)

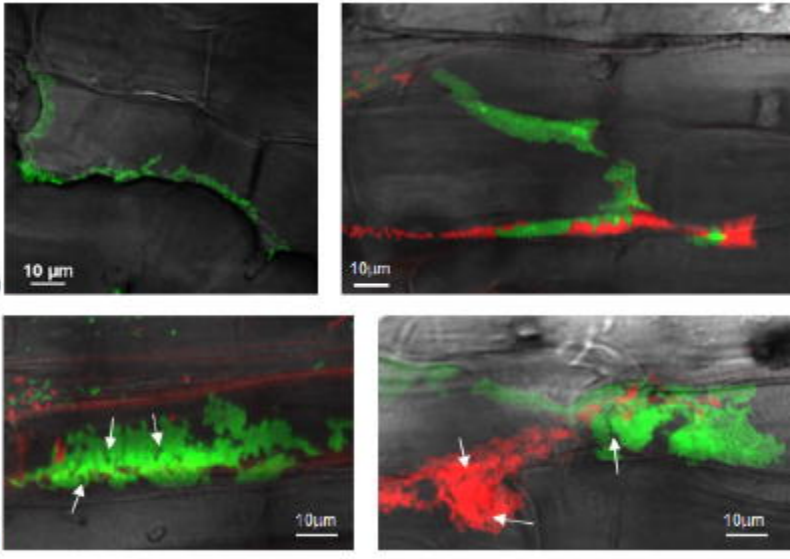
(a)
10 µm
10µm
(b)
10µm
10µm

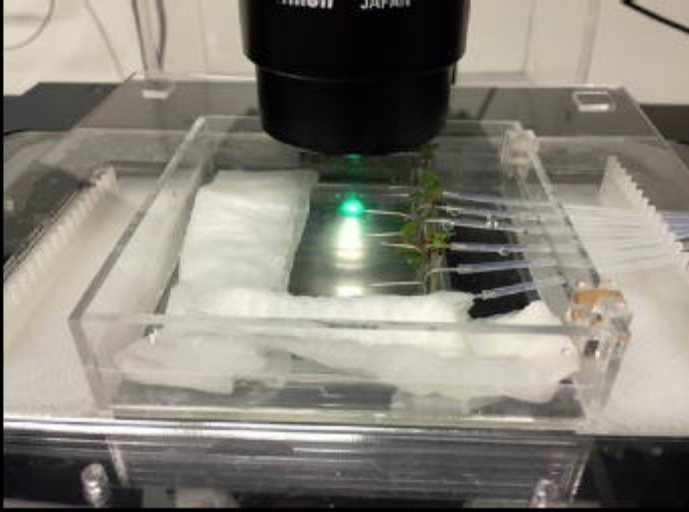
JAPAN

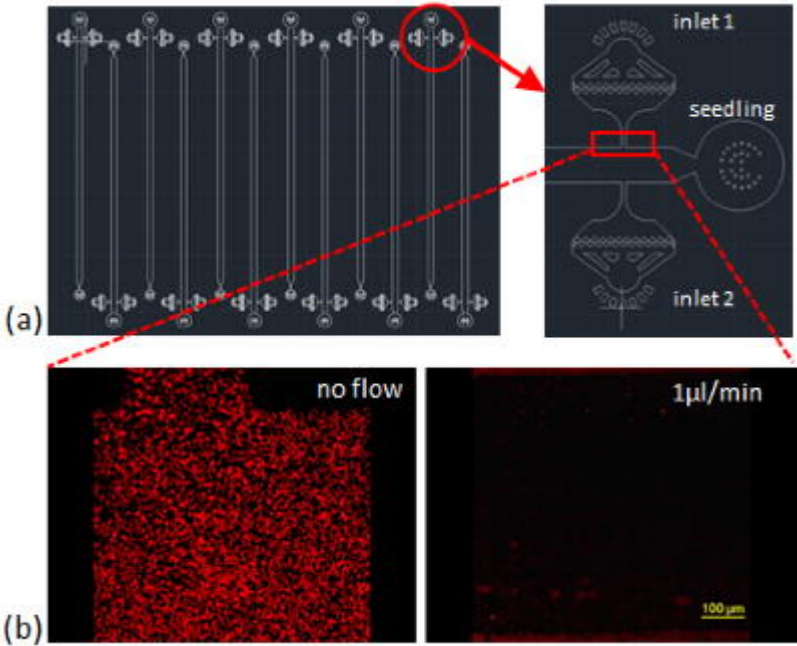
inlet 1
seedling
inlet 2
(a)
no flow
1µl/min
100 µm
(b)